



Evolution of residual stresses with fatigue crack growth in integral structures with crack retarders

C.D.M. Liljedahl, M.E. Fitzpatrick*, L. Edwards¹

Materials Engineering, The Open University, Walton Hall, Milton Keynes, MK7 6AA, UK

ARTICLE INFO

Article history:

Received 16 February 2009

Received in revised form 21 May 2009

Accepted 12 June 2009

Keywords:

Residual stresses

Neutron diffraction

Finite element analysis

Fatigue

Crack retarders

Hybrid structures

ABSTRACT

Bonded straps are investigated for their ability to retard a growing fatigue crack in metallic structures. The evolution of the residual stresses in the vicinity of the strap with fatigue crack growth has been studied. Cracks were grown in single edge-notched tension (SEN(T)) specimens reinforced with either a titanium or a carbon fibre reinforced plastics (CFRP) strap. The residual stress evolution has been measured *in situ* during crack growth using neutron diffraction, and modelled with a finite element approach. The peak residual stresses induced by the mismatch of the coefficient of thermal expansion between the strap and plate materials were seen to be fairly constant with crack growth. Good correlation between the experimental and the modelling results was found, except at very long crack lengths for a specimen that exhibited considerable fracture surface roughness at long crack lengths. The difference was attributed to wedging of the fracture surface changing the expected stress state, rather than any effect of the strap.

© 2009 Elsevier B.V. All rights reserved.

1. Introduction

The use of integral structures can potentially reduce the weight and the cost of aerospace assemblies. An inherent inconvenience with integral structures is, however, that there are no natural crack stoppers as there are in riveted structures. Large safety factors therefore have to be applied to integral structures if they are to comply with airworthiness regulations. This then reduces the weight competitiveness of metallic integral structures as compared with other technologies such as fibre reinforced polymer composites.

The research presented here is part of a project to investigate the role of adhesively bonded reinforcements in improving the damage tolerance characteristics of integral structures. This concept has been tested successfully on coupon specimens and a significant life extension was obtained [1].

The reinforcement, which is usually present in the form of an elongated plate or 'strap', should have a reasonably high strain to failure, high strength and good fatigue resistance. In order to achieve these properties at minimal additional weight, this implies that a different material than that of which the integral structure is made will be used for the reinforcing strap. As the bonding adhesive used to affix the strap will be cured at an elevated tem-

perature, when the structure subsequently cools residual stresses are induced due to the mismatch of coefficient of thermal expansion between the integral structure and the strap. These residual stresses can be deleterious to fatigue crack initiation and growth in the structure. It has been found that these cure-induced residual stress have a significant effect on the fatigue crack growth rate in selectively reinforced structures [2]. Hence in order to be able to design an optimal structure without having to use severely conservative safety factors, the residual stresses have to be measured to be able to develop and verify predictive models. Measurements of the induced residual stresses in structures reinforced with candidate strap materials have previously been carried out at room temperature [3,4]. Good correlation was found between the measurement and a finite element simulation of the cure-induced stresses.

In this work the evolution of the residual stress with fatigue crack growth has been measured with neutron diffraction and modelled with a finite element approach.

2. Experimental procedures

2.1. Specimens

Single edge-notched tension (SEN(T)) specimens were sectioned from a 10 mm-thick aluminium alloy 7085-T7651 plate. The final length was 400 mm and the width was 140 mm (Fig. 1). The assembly was bonded with FM[®] 94 adhesive supplied by Cytec Ltd. [5], and cured at 120 °C for 1 h with an applied pressure of 0.28 MPa.

* Corresponding author. Tel.: +44 1908 653100; fax: +44 1908 653858.

E-mail address: M.E.Fitzpatrick@open.ac.uk (M.E. Fitzpatrick).

¹ Current address: Institute of Materials Engineering, ANSTO, PMB1, Menai, NSW 2234, Australia.

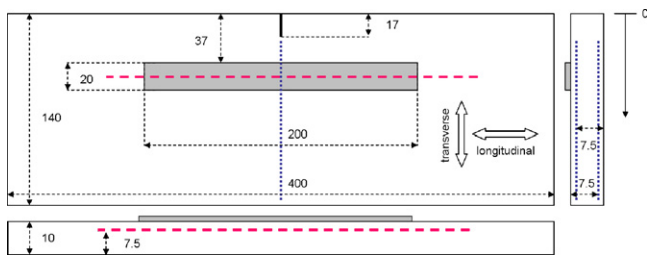


Fig. 1. Specimen geometry and strap position. The SEN(T) sample was 10 mm thick and the straps were 2 mm thick. Residual strains were measured 2.5 and 7.5 mm below the surface to which the strap was bonded, along the lines shown, along the crack growth direction; and 2.5 mm below the strap surface along the strap length.

The samples were prepared at Cranfield University. The material properties used in the following analyses are given in Table 1.

Two specimens were tested, one with a titanium strap and one with a carbon fibre reinforced plastics (CFRP) strap. Both straps were 2 mm thick. The strap dimensions and the position of the strap can also be seen in Fig. 1. Before bonding, the aluminium alloy was acid etched for the specimen bonded with a titanium strap and acid etch anodized for the specimen bonded with a CFRP strap.

2.2. Residual stress measurement and in situ fatigue

Neutron diffraction is an established non-destructive technique to determine strains within structures [6]. The inter-planar lattice spacing for various crystal reflections can be determined from the position of the diffraction peaks as realized by Bragg [7]. The inter-planar lattice spacing can be used, in conjunction with a 'stress-free' value of the lattice parameter, to determine the internal strains in the material, which can then be used to calculate the internal stresses.

The measurements were carried out on the ENGIN-X diffractometer in the UK [8] and the SALSA diffractometer in France [9].

ENGIN-X is based at the ISIS pulsed neutron source at the Rutherford Appleton Laboratory, Didcot, UK. The instrument has two detector banks at $\pm 90^\circ$ to the incident beam, which allows for strain measurements in two directions simultaneously. The broad wavelength range of neutrons in each pulse allows for the measurement of several peaks in the diffraction spectrum simultaneously. A servohydraulic Instron 100 kN stress-rig was placed onto the sample table and the specimen was fatigue loaded *in situ* (Fig. 2).

SALSA is located at the Institut Laue Langevin (ILL) neutron source in Grenoble, France and is a constant wavelength diffractometer. The (3 1 1) diffraction plane was measured as it gives a high multiplicity and high intensity.

The specimen bonded with a titanium strap was measured at ENGIN-X. Before the start of the measurement of the specimen, the crack had been initiated to a length of 29 mm. The applied nominal stress to initiate the crack was 64 MPa (90 kN) with $R=0.1$ at a frequency of 10 Hz. The loads were progressively reduced with crack growth using the ΔK -decreasing procedure described in ASTM E647 [10], until a final nominal stress of 19 MPa was achieved at a crack length of 29 mm. The first residual stress measurement

Table 1

Material properties: the subscript indicates fibre direction parallel (1) and perpendicular (2) to the fibre direction respectively, for the metals isotropic material properties are assumed; E is elastic modulus, G is shear modulus, ν is Poisson's ratio and α is coefficient of thermal expansion.

Material	E_1 (GPa)	E_2 (GPa)	G_{12} (GPa)	ν_{12}	α_1 (μK^{-1})	α_2 (μK^{-1})
7085-T7651	71	71	27	0.33	23.6	23.6
CFRP	135	5.7	4.0	0.28	−0.3	30.0
Ti6Al4V	114	114	42	0.34	8.6	8.6

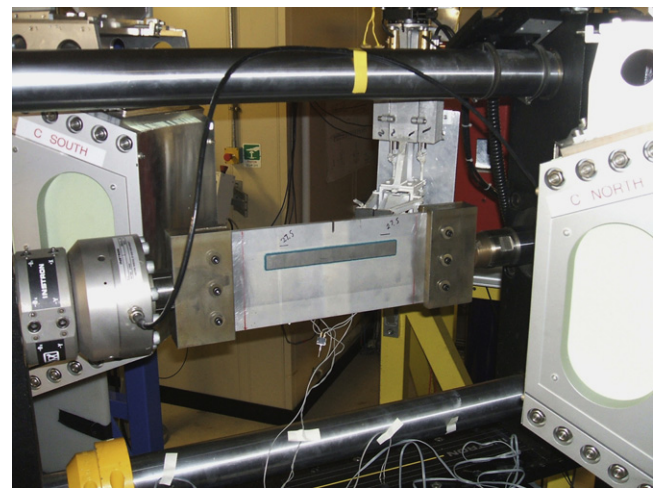


Fig. 2. Set-up at the ENGIN-X diffractometer (for measurement of the sample reinforced with a titanium strap).

was undertaken on the specimen with a crack length of 29 mm, and from this crack length the specimen was loaded *in situ* on the diffractometer under a constant cyclic load of 26 kN (19 MPa) with a frequency of 20 Hz and a stress ratio R of 0.1. The residual stresses were measured at intervals of crack length, until a crack length of 93.5 mm was reached whereupon the crack turned and the strap debonded.

The specimen bonded with a CFRP strap was measured on the SALSA diffractometer. The crack was initiated *in situ* at a maximum load of 45 kN (32 MPa) with a stress ratio $R=0.1$ until a crack length of 24 mm was reached. Thereafter the maximum load was kept at 26 kN (19 MPa) and a stress ratio $R=0.1$ as for the other specimen. The frequency was 20 Hz. A stress measurement was performed before the crack was initiated for this specimen.

For both the set-ups the measurements were carried out along the crack growth direction at two positions (2.5 and 7.5 mm from the bonded side) through the thickness (Fig. 1).

The gauge volume over which the measured strain is averaged is defined by slits or collimators on the incident beam, and also by the divergence of the beam. At ENGIN-X the incoming slit was 2 mm wide and the height was set to 5 mm, and collimators with a full-width at half-maximum (FWHM) spread of 2 mm were used in front of the detector banks. The horizontal divergence of the beam is about 2.5 mrad. The distance of the slit to the centre of the gauge volume was approximately 100 mm so this increases the horizontal beam dimension by approximately 0.25 mm. The vertical divergence is approximately 10 mrad and hence this adds 1 mm to the vertical gauge volume dimension. The outgoing beam is a function of the FWHM of the collimator resolution function. For the 2 mm collimators this will add 0.5 mm on either side.

At SALSA the height of the slit was set to 2.5 mm and the width to 2 mm. The divergence multiplication factor is about 2.5 in the vertical and about 1.4 in the horizontal direction for a slit position about 100 mm from the gauge centre and for this set-up.

The longer dimension was oriented in the crack growth direction for both specimens and set-ups. A short gauge dimension had to be used in the thickness direction of the plate as the stress state is mainly out-of-plane bending.

Pawley refinement [11] was used to determine the lattice parameters for the measurements carried out at ENGIN-X: this has been shown to yield a good approximation of the engineering strain in the component [12]. EX-SBA, the ENGIN-X Script Based Analysis software, was used for the data analysis. A cube measuring 10 mm \times 10 mm \times 10 mm was used to provide stress-free reference

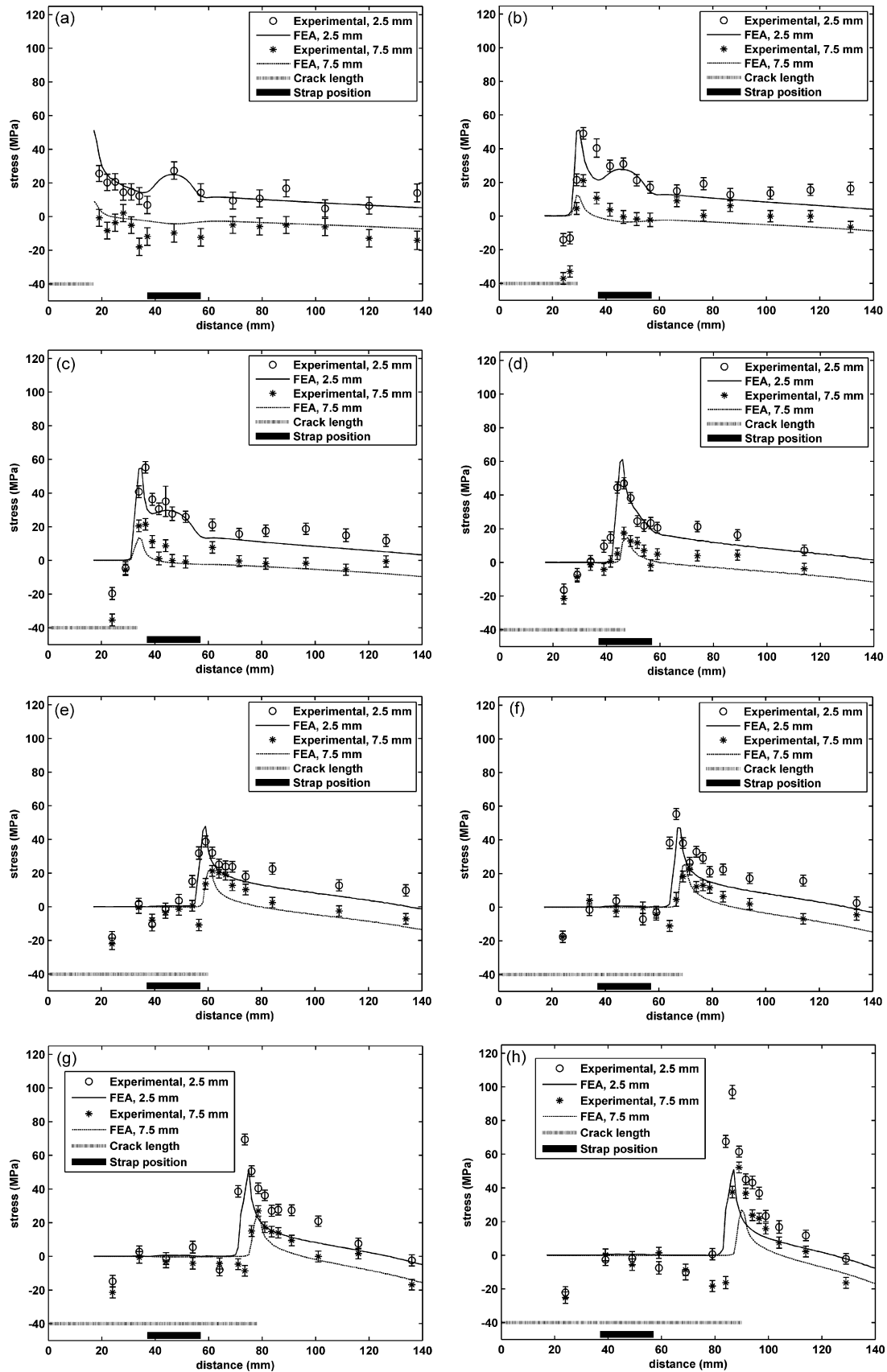


Fig. 3. Evolution of residual stresses in the longitudinal stress direction that acts perpendicular to the notch (see Fig. 1) in the specimen bonded with a titanium strap for a crack length of (a) 17 mm (here only a notch was present and no crack, this data was measured during another work and is published elsewhere [3]), (b) 29.5 mm, (c) 33.5 mm, (d) 47 mm, (e) 60 mm, (f) 69 mm, (g) 78 mm and (h) 90 mm.

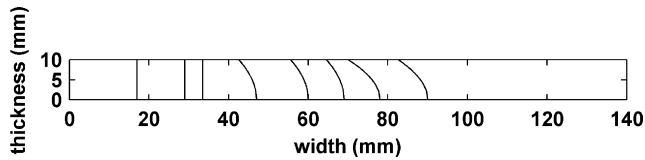


Fig. 4. Evolution of the crack front with crack length in the specimen bonded with a titanium strap.

values of lattice parameter in the computation of the macrostrain. This cube was measured in all three directions to be able to account for any intergranular anisotropy induced during the rolling of the plate. The strain in each measured direction was hence computed using the following relation

$$\varepsilon = \frac{a_{\sigma} - a_0}{a_0} \quad (1)$$

where a_{σ} represents the value of the lattice parameter in the SEN(T) sample and a_0 is the value of the lattice parameter in the cube.

The strain was computed in a similar way for the diffraction results obtained at SALSA, but here the lattice spacing for the (3 1 1) plane was used instead of the Pawley-determined lattice parameter obtained at ENGIX. The (3 1 1) lattice reflection is known to give good representation of the average lattice strain in the measured gauge volume [13].

The orientation of the sample as fixed in the stress-rig allowed for measurement in the longitudinal and the normal strain directions. From prior experiments on SEN(T) samples reinforced with titanium straps it was found that the stresses in the normal direction were very small [4]. Plane stress was hence assumed in the computation of the residual stresses using Hooke's law.

The crack length was measured, on the un-bonded side, using fractomat gauges (FAC-20, Tokyo Sokki Kenkyojo Co. Ltd.).

2.3. Crack front

The specimen is asymmetric as it is only reinforced on one side. A fatigue crack will propagate faster on the un-reinforced side. The crack fronts in asymmetric repair specimens tested by Seo and Lee [14] and Hosseini-Toudeshky and Mohammadi [15] appear to be essentially parabolic in shape. In the present work, only the crack length on the un-bonded side was measured. In order to estimate the shape of the crack front at the measured crack lengths a

parabolic shape was assumed, i.e.

$$c = c_{un} - \frac{y^2}{4p} \quad (2)$$

where c is the crack length at a position y through the thickness for a certain measured crack length at the un-bonded side (c_{un}); p is a constant.

The positions of the peak residual strains in the longitudinal direction at the two measured positions through the thickness were taken as an estimation of the crack tip position at these points through the thickness. The constant p was hence determined by a least squares fit of the above equation of these values.

2.4. Debond

In order to be able to estimate the extent of any debond of the adhesive layer with fatigue the residual strains were also measured as a function of position along the length of the strap (Fig. 1), 2.5 mm below the bond line. Debonding was assumed to have taken place if a reduction of the residual strain compared to the un-cracked condition was observed.

3. Finite element modelling

The temperature at which the thermal residual stresses become zero upon re-heating after cure is referred to as the stress-free temperature (T_{sf}). The stress-free temperature often coincides with the glass transition temperature (T_g) [16] if the adhesive is cured above T_g . For a system where T_g is above the curing temperature, T_{sf} is taken to be equal to the curing temperature (T_c) [17]. Hence, in this work the induced thermal residual stresses have been modelled applying the temperature drop defined below, since the T_g [6] nearly coincides with the curing temperature (T_c):

$$\Delta T = T_c - T_{RT}$$

All the finite element modelling was carried out using the commercial finite element package ABAQUS. The linear elastic material properties given in Table 1 were used in the analysis. Non-linear geometry effects were accounted for. The aluminium base plate was modelled with 20-node reduced integration elements (C3D20R) and the thin layer of adhesive and the strap was modelled with 8-node reduced integration continuum shell elements (SC8R). The elements were 1.25 mm × 2.5 mm × 2.5 mm in the plate and 1.25 mm × 1.25 mm in the adhesive and the strap

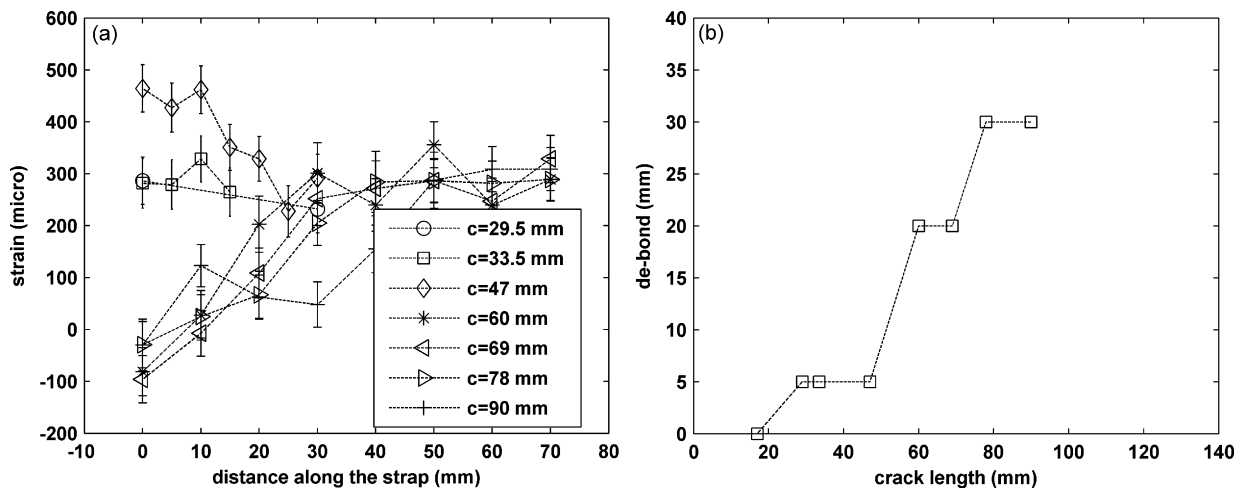


Fig. 5. (a) The variation of residual strain along the strap length (longitudinal direction), 2.5 mm below the plate surface as shown in Fig. 1, as a function of crack growth, showing relaxation of the stress in the strap as the crack length increases (b) the estimated debond using these data.

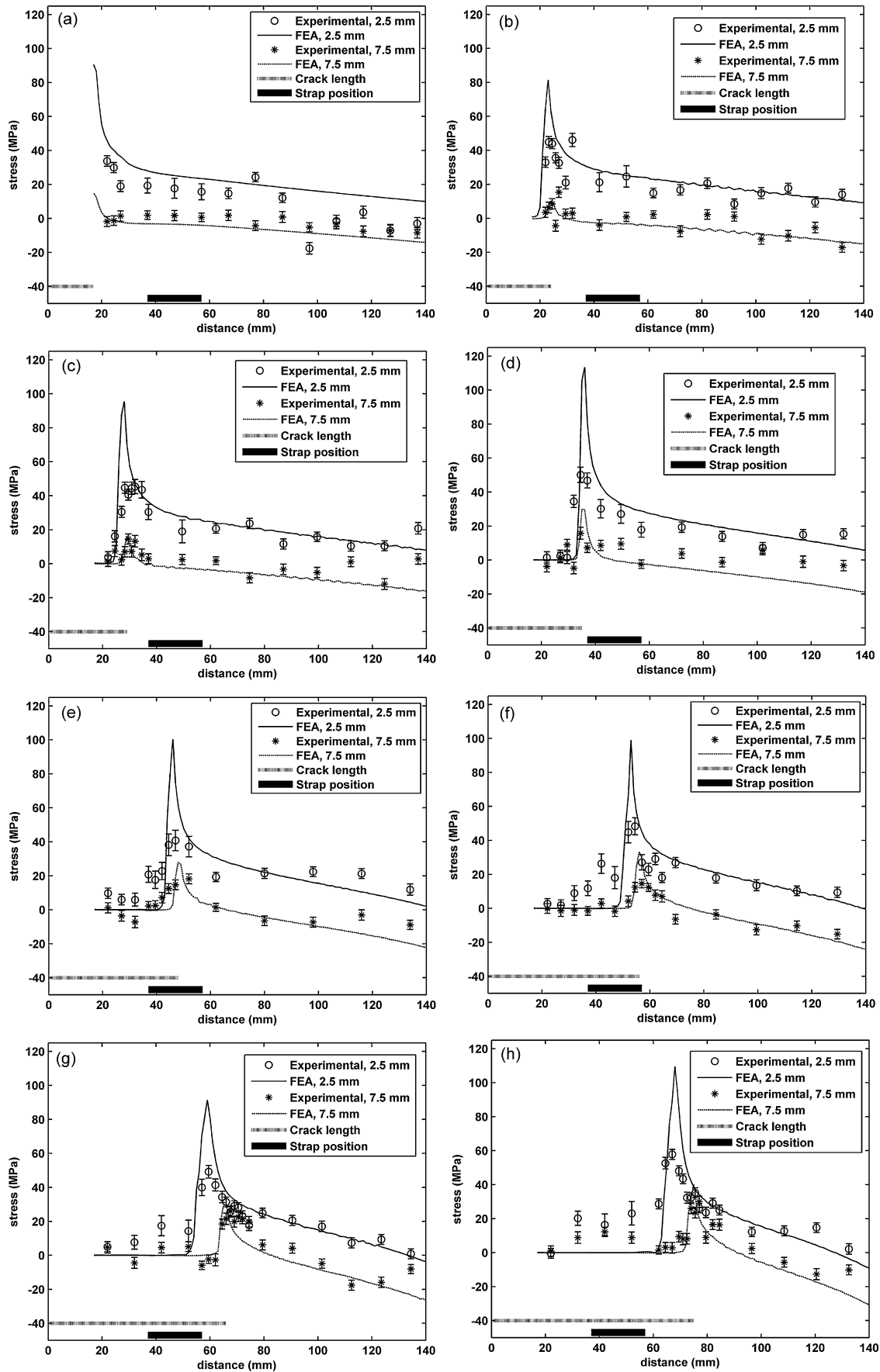


Fig. 6. Evolution of residual stresses (in the longitudinal stress direction that acts perpendicular to the notch; see Fig. 1) in the specimen bonded with a CFRP strap for a crack length of (a) 17 mm (here only a notch was present), (b) 24 mm, (c) 29 mm, (d) 35 mm, (e) 48 mm, (f) 56 mm, (g) 66 mm, (h) 75 mm, (i) 85 mm, (j) 93.5 mm and (k) 105 mm.

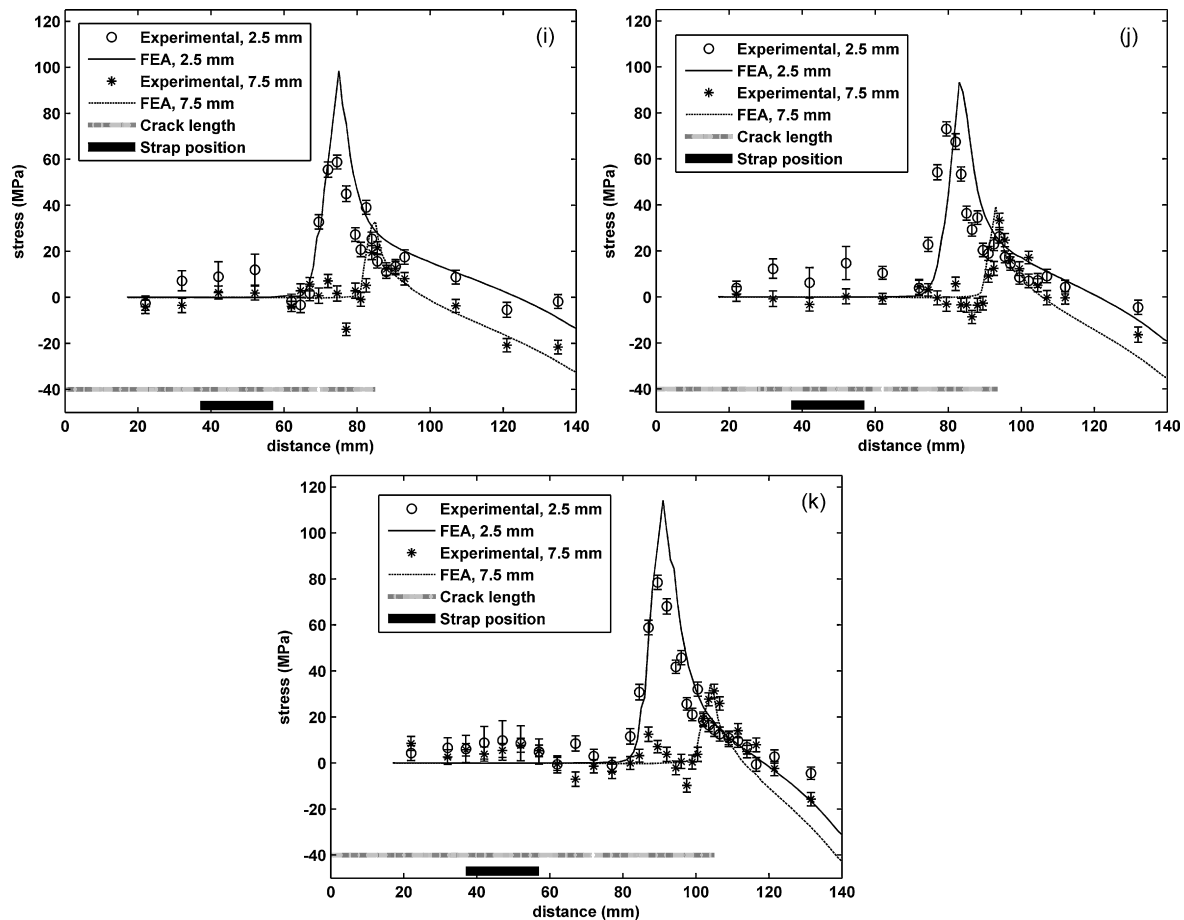


Fig. 6. (Continued).

away from the crack tip. Smaller elements were used in the adhesive and the strap to assure that the nodal density between the plate and the adhesive were similar. Closer to the crack tip the mesh was refined with smaller elements of a size of approximately $1.25 \text{ mm} \times 0.6 \text{ mm} \times 0.6 \text{ mm}$. The surfaces between the plate and the adhesive, and the adhesive and the strap, were bonded together using surfaced based constraints. The degrees of freedom on the slave surface are eliminated and the nodes are set to deform as the closest node on the master surface using the TIE option in ABAQUS.

The actual neutron gauge volume was approximately $6 \text{ mm} \times 2.5 \text{ mm} \times 2.5 \text{ mm}$ for both set-ups. Hence in order to be able to compare the numerical results with the experimental results, the numerical results were also averaged over the equivalent volume.

The crack front was modelled with the shape of the estimated shape as discussed in Section 2.3. The debond for each crack length was also set to a length as explained in Section 2.4.

4. Results

4.1. Ti strap

The evolution of the residual stresses in the specimen bonded with a titanium strap can be seen in Fig. 3. Only the stresses which contribute to opening of the crack in mode I (the longitudinal strains as defined in Fig. 1) are presented to save space.

The evolution of the crack front determined as described in Section 2.3 can be seen in Fig. 4.

The evolution of the residual strain along the length of the strap (2.5 mm below the plate surface as indicated in Fig. 1) with crack length, and the consequent estimation of the degree of debond, as explained in Section 2.4, can be seen in Fig. 5a and b.

At a crack length of about 93.5 mm the strap debonded completely. The specimen was removed from the grips and the specimen was measured again, to verify that the gripping did not induce any additional stress into the sample.

4.2. CFRP strap

The evolution of the residual stresses in the specimen bonded with a CFRP strap can be seen in Fig. 6. Also here only the stresses in the longitudinal direction are presented to save space.

The evolution of the crack front determined as described in Section 2.3 can be seen in Fig. 7.

The evolution of the residual strain along the extension of strap as seen in Fig. 1 and the consequent estimation of the degree of debond, as explained in Section 2.4, can be seen in Fig. 8.

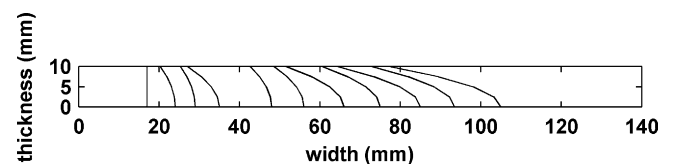


Fig. 7. Evolution of the crack front in the specimen bonded with a CFRP strap.

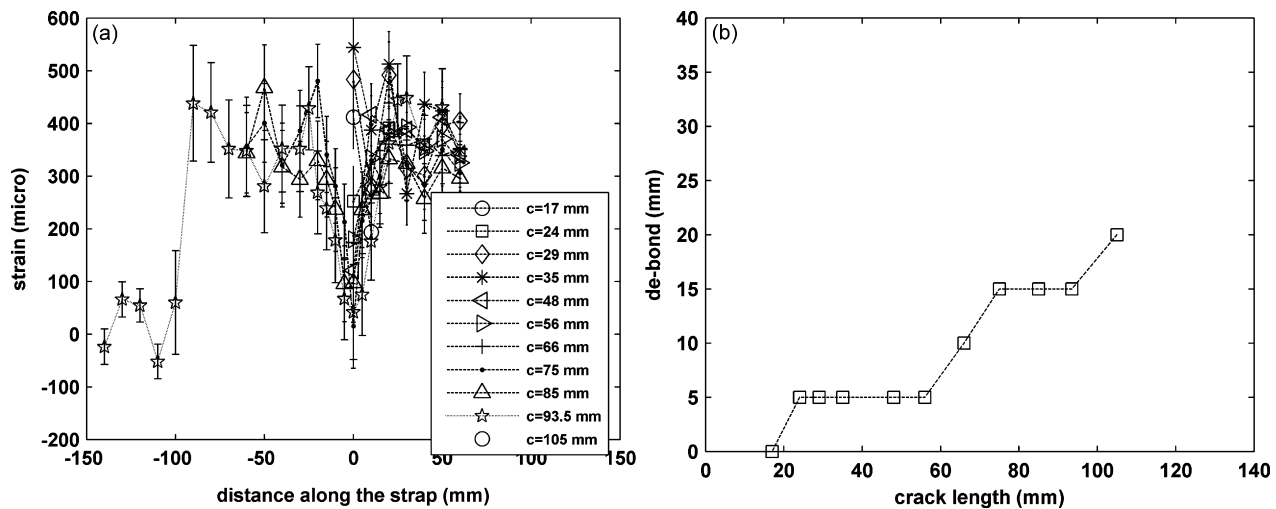


Fig. 8. (a) The variation of residual strain along the CFRP strap length as a function of crack growth, showing relaxation of the stress in the strap as the crack length increases and (b) the estimated debond using these data.

5. Discussion

In Fig. 3a the initial stress state in the specimen before any load cycles had been applied is shown. In this figure it can be seen that, apart from the higher stresses (compared with most of the other positions along the measured path) at the stress concentration at the initial notch tip, higher stresses are also found at the position under the strap. The peak stresses at the strap arise as the strap constrains the specimen in both the longitudinal and the transverse direction. This is explained further elsewhere [3,4]. In Fig. 3b the residual stress state after crack initiation is shown, and it can be seen that the peak stress moves from the notch tip to the current crack tip at about 29 mm. The compressive stresses behind the crack tip might be due to crack closure; it was observed that the fracture surface was quite rough where the crack initiation had been carried out. The further evolution of the crack tip can be seen in the following figures (Fig. 3c–h). There is a reasonable correlation between the experimental and the numerical results for Fig. 3a–e. In Fig. 3f–h it can be seen that the stresses are underestimated by the model. It is important to point out that the overall profile should be compared and not just the peak stresses: the peak stresses are very sensitive to the size of gauge volume used in the averaging of the numerical data. The underestimation appears at long crack lengths, and it was observed post-failure that the crack surfaces became rougher at longer crack lengths. This rough surface might hence act as a wedge, increasing the residual stresses. In the FE model, only residual stresses due to the constraints of the strap, and a flat fracture surface, were considered (i.e., no roughness effects). The residual stresses present after the strap debonded are also consistent with the rough fracture surface at long crack length acting as a wedge and inducing significant residual stresses. The wedging is hence a plausible explanation for the mismatch between the experimental and numerical data at long crack lengths.

The un-fatigued residual stress state in the specimen reinforced with a CFRP strap is shown in Fig. 6a. Here no increase in residual stress is seen at the position of the strap, as the stiffness in the transverse direction of this unidirectional CFRP strap is small compared with the stiffness of the aluminium plate. Further details can be found elsewhere [3,4]. The evolution of the residual stress with crack length can be seen in the following figures (Fig. 6b–k). Apart from the peak stresses there is a reasonable correlation between the experimental and numerically determined profiles for all crack lengths. No significant difference between the experimental and modelled data can be seen at long crack lengths, as was the case for

the specimen bonded with a titanium strap. It was observed post-fracture of the specimen that the fracture surface was less rough as compared with the specimen bonded with a titanium strap. It can also be observed that the tensile residual stresses are initially larger in the specimen bonded with a CFRP strap at the start of the test, and the peak crack tip stresses are larger as the crack grows. Both these effects imply that the wedging will be much lower for the specimen bonded with a CFRP strap (as tensile stress opens the crack).

The estimated evolution of the crack front can be seen in Figs. 4 and 7 for the specimen bonded with a titanium strap and a CFRP strap respectively. Comparing these figures it can be seen that the crack front is much more skewed in the specimen bonded with a CFRP strap. The CFRP strap is much stiffer, and hence there is a larger difference between the retardation on the bonded compared to the un-bonded side. A larger debond was found for the specimen with a titanium strap (Figs. 5 and 8). This effect is important to consider as the size of the debond influences considerably the effectiveness of the retardation; however no firm conclusions can be drawn in this case as the two specimens had difference surface preparations: the specimen with a titanium strap was acid etched and the specimen with a CFRP strap was acid-etched and anodised.

The specimen with the CFRP strap had a longer crack growth life despite the higher residual stresses. The overall effectiveness of the strap is a combination of the stiffness ratio (the additional stiffness provided by the strap), the extent of debond when the crack grows below the strap, and the effect of the residual stresses. The stiffness is higher and the debond is lower in the specimen bonded with a CFRP strap, so even though the residual stresses are higher than in the specimen bonded with a titanium strap the bridging, and hence the reduction of the effective ΔK , will be much higher in that specimen than the specimen bonded with a titanium strap.

At short to intermediate crack lengths the residual stresses are governed by the initial thermal residual stresses, as the fracture surface is smooth and there is minimal wedging. Due to the smaller residual stresses in the titanium strap there will be less thermal opening of the crack at zero applied external load, and hence the wedging (closure) will be higher in this specimen than in the specimen with the CFRP strap at long crack lengths. In the specimen bonded with a CFRP strap the tensile thermal stresses cause greater opening of the crack, reducing contact between the fracture surfaces and hence causing less closure. Hence although the residual stresses due to the bonding of the strap are higher in the specimen with a CFRP strap, at long crack lengths the closure in the titanium

specimen will produce larger residual stresses than in the CFRP sample. The thermal tensile residual stresses speed up the crack growth (higher R), while the closure reduces the effective ΔK .

6. Conclusions

- (1) The residual stresses associated with crack-retarding straps have been measured using neutron diffraction. The evolution of the residual stresses as a growing fatigue crack passes the strap have been measured experimentally and modelled using the finite element method.
- (2) The strap provides a bridging effect to the fatigue crack wake, although there is progressive debonding of the strap as the crack length increases beyond the strap.
- (3) Good correlation was obtained between the measured and modelled stresses, showing that an elastic model gives accurate estimates of the evolution of the residual stresses at low to medium applied stresses intensity factors. The residual stresses can hence be included directly in a linear-elastic fracture mechanics (LEFM) modelling approach when predicting the behaviour of hybrid structures.
- (4) The model predictions worsened at very long crack lengths when the crack surface was noticeably rough, and additional wedging of the crack had occurred.

Acknowledgements

The authors gratefully acknowledge Dr Ed Oliver at ENGIN-X, ISIS and Dr Darren Hughes at SALSA, ILL for help during the experiments. The specimens were prepared at Cranfield University, and Professor Phil Irving is thanked for his part in the collaboration. Alcoa and Airbus UK are gratefully acknowledged for financial support of this project, and Dr Markus Heinemann and Gerry Shepherd are thanked

for their comments on the draft of this paper. MEF is supported by a grant through The Open University from the Lloyd's Register Educational Trust, an independent charity working to achieve advances in transportation, science, engineering and technology education, training and research worldwide for the benefit of all.

References

- [1] X. Zhang, M. Boscolo, D. Figueroa-Gordon, G. Allegri, P.E. Irving, *Engineering Fracture Mechanics* 76 (2009) 114–133.
- [2] P. E. Irving, D. Figueroa-Gordon, Routes to improved damage tolerance; prediction of damage tolerant performance of high strength and hybrid structures, in *First International Conference on Damage Tolerance of Aircraft Structures* R. Benedictus, J. Schijve, R.C. Alderliesten, J.J. Homan (eds.), Delft, Holland, 2007, <http://dtas2007.fyper.com/userfiles/file/Paper%2054.Irving.pdf>, Accessed April 2009.
- [3] C.D.M. Liljedahl, M.E. Fitzpatrick, L. Edwards, *Composite Structures* 86 (2008) 344–355.
- [4] C.D.M. Liljedahl, M.E. Fitzpatrick, L. Edwards, *Materials Science and Engineering* 486 (2008) 104–111.
- [5] FM(r) 94 Modified Epoxy Film Datasheet. http://www.cytec.com/engineered-materials/products/Datasheets/FM_94.pdf, Accessed July 7th 2009.
- [6] M.E. Fitzpatrick, A. Lodini, *Analysis of Residual Stress using Neutron and Synchrotron Radiation*, Taylor & Francis, London, 2003.
- [7] W.L. Bragg, *Proceedings of the Philosophical Society* 17 (1914) 43–57.
- [8] J.R. Santisteban, M.R. Daymond, J.A. James, L. Edwards, *Journal of Applied Crystallography* 39 (2006) 812–825.
- [9] T. Pirling, G. Bruno, P.J. Withers, *Materials Science and Engineering: A* 437 (2006) 139–144.
- [10] E647–88a, ASTM, 1990.
- [11] G.S. Pawley, *Journal of Applied Crystallography* 14 (1981) 357–361.
- [12] M.R. Daymond, M.A.M. Bourke, R.B.V. Dreele, B. Clausen, T. Lorentzen, *Journal of Applied Physics* 82 (1997) 1554–1562.
- [13] B. Clausen, T. Lorentzen, T. Leffers, *Acta Materialia* 46 (1998) 3087–3098.
- [14] D.-C. Seo, J.-J. Lee, *Composite Structures* 57 (2002) 323–330.
- [15] H. Hosseini-Toudeshky, B. Mohammadi, *Composite Structures* 79 (2007) 234–241.
- [16] J. Kuczynski, A.K. Sinha, *IBM Journal of Research & Development* 45 (2001) 783–788.
- [17] H.E. Bair, D.J. Boyle, J.T. Ryan, C.R. Taylor, S.C. Tighe, D.L. Crouthamel, *Polymer Engineering & Science* 30 (1990) 609–617.